Catalysis Letters Vol. 109, Nos. 1–2, June 2006 (© 2006)
DOI: 10.1007/s10562-006-0062-6

Bulk and surface properties of a VPO catalyst used in an electrochemical membrane reactor: conductivity-, XRD-, TPO- and XPS-study

L.K. Rihko-Struckmann,[a,*] Y. Ye,[a] L. Chalakov,[b] Y. Suchorski,[b] H. Weiss,[b] and K. Sundmacher[a,b]

[a]*Max Planck Institute for Dynamics of Complex Technical Systems, Sandtorstr. 1, Magdeburg D-39016, Germany*
[b]*Otto-von-Guericke University Magdeburg, Universitätsplatz 2, Magdeburg D-39016, Germany*

Received 3 January 2006; accepted 26 January 2006

In the first part of this work, the electrical conductivity of vanadium phosphorous oxide (VPO) catalyst was investigated by means of the 2-probe EIS method. The VPO showed an extremely low conductivity at low oxygen partial pressure, which is the prevailing condition in the anodic compartment in an electrochemical membrane reactor (EMR). In the second part of this study, fresh as well as VPO catalyst already used in an EMR were characterised with XRD, XPS and temperature programmed oxidation (TPO). The XRD measurements revealed an unchanged bulk phase structure after operation in the EMR. Significant differences in the average oxidation states of vanadium in the catalyst layer in the EMR were determined via XPS, where the catalyst surface facing the electrolyte membrane was more oxidised than the surface facing the anodic gas compartment. The lowered uptake and release of oxygen was observed in TPO experiments for the catalyst used in the EMR.

KEY WORDS: vanadium phosphorous oxide; electrochemical membrane reactor; butane oxidation; electrical conductivity; oxidation state.

1. Introduction

The oxidation of butane to maleic anhydride (MA), which is catalysed by vanadium phosphorous oxide (VPO), is so far the only successful direct oxidation process of light hydrocarbons on the industrial scale. Due to the importance of the butane oxidation process, and the complex nature of the VPO catalysts, their physical and chemical properties have been intensively characterised during the last years, as recently reviewed by Hutchings [1]. In order to increase the process selectivity, numerous modifications for the catalyst synthesis have been proposed [2–4], and various reactor concepts have been investigated. Spatially separated reduction and oxidation steps for the catalyst have been demonstrated in the riser-regenerator recirculating configuration by Dupont [5]. Santamaria and coworkers investigated a new process configuration, a packed bed membrane reactor, for the production of MA [6,7]. Besides this porous membrane reactor concept, solid electrolyte membrane processes can also be an interesting option for the production of chemicals [8]. The feasibility of butane oxidation in a tubular electrochemical membrane reactor (EMR) using a VPO catalyst layer on an anodic electrode has been recently investigated (for a schematic illustration of the EMR, see figure 1) [9,10]. In the EMR, oxygen is reduced at the cathode and transferred through an oxygen ion conducting solid electrolyte membrane to the anode, where it can either react with hydrocarbons or form gaseous molecular oxygen. The oxygen flux through the membrane is controlled by either the electric current (galvanostatic mode) or the electric potential (potentiostatic mode).

In the first part of the present study, the total electrical conductivity of VPO was investigated under various process conditions. This information is required for the improvement of the anodic electrode/catalyst design in the EMR. High ionic conductivity is required for efficient oxygen ion transfer as the oxygen ions diffuse from the electrolyte membrane surface to the reaction zone. Since the electrons, released during the anodic oxidation, have to be conducted to the external electrical circuit, high electronic conductivity of the catalyst is needed as well. Only a catalyst material with high ionic and electronic conductivities can simultaneously serve as a conductor in the EMR and can enable the reaction to occur over the entire catalyst surface being in contact to gas phase butane. If electronic and/or the ionic conductivity of the catalytically active material are low, the composition of the catalyst/electrode layer is more complicated, as separate conductors for ion and electron transfer on the anode are necessary in order to provide a sufficient reaction zone.

In the second part of the present investigation, surface area, phase structure, chemical composition and in particular the oxidation state of the VPO catalyst were characterised before and after operation in the EMR. In

*To whom correspondence should be addressed.
E-mail: rihko@mpi-magdeburg.mpg.de

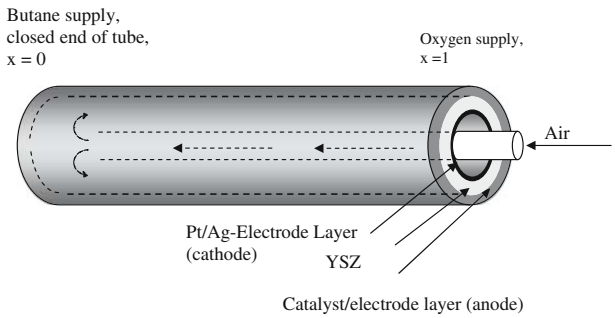

Figure 1. Schematic illustration of the tubular electrochemical membrane reactor. Air supply to the inner part of the yttria-stabilised zirconia tube (YSZ), anodic electrode and VPO layer on the outer surface of the YSZ tube.

a previous investigation of the butane partial oxidation in an EMR, a slow catalyst deactivation was observed [9]: the selectivity to MA was slightly decreasing during several hours of operation, while the selectivity to carbon oxides, especially to CO_2 was increasing [11]. It is well known that the VPO catalyst is highly sensitive to the operating conditions, and needs a long equilibration period in order to reach the maximum activity [12]. A high operating temperature is desired in the EMR in order to obtain high oxygen flux through the electrolyte membrane. On the other hand, a low operating temperature (below 673 K) is favourable for the catalyst selectivity. Due to this selectivity limitation, the EMR has to be operated at moderate temperatures (below 823 K), and therefore the oxygen/butane ratio in this process (between 0.2 and 1.4 in the temperature range from 723 to 783 K [9]) is lower than in the conventional gas phase process. In turn, it is to be expected that the low oxygen/butane ratio and the high temperature level lead to a changed VPO catalyst composition during the operation, and possibly a different selectivity. For this reason, the VPO catalysts were characterised before and after operation in the EMR by means of the techniques given below.

2. Experimental

The VPO catalyst precursor was prepared from V_2O_5 and H_3PO_4 with isobutanol by the one-step organic synthesis route published by Johnson *et al.* [13], and described in detail in [9]. The conversion of the precursor material $VOHPO_4 \cdot 0.5H_2O$ to the activated VPO was carried out in three steps: treatment in nitrogen at 823 K for about 40 h, calcination in air at 673 K for 1 h, and activation with 1.0 vol% butane in air at 673 K for 2 h.

2.1. Conductivity measurements

For the conductivity measurements, catalyst discs with 13 mm in diameter and 1 mm thickness were prepared by pressing ~300 mg of precursor powder at 10 MPa. Platinum electrodes of 1 μm thickness were deposited by physical vapor deposition (PVD) on both flat surfaces of the discs, using dc-magnetron sputtering with a Pt target (purity 99.95%) in a high vacuum coating system MED 020 (BAL-TEC, Liechtenstein). The precursor discs were converted to the activated VPO catalyst as described above.

The conductivity of the VPO discs was measured by 2-probe electrochemical impedance spectroscopy (EIS). AC impedance spectra were recorded using an IM6 Impedance Analyzer (Zahner Electric, Germany) at open circuit voltage by sweeping the frequencies between 1 Hz and 1 MHz, recording 10 points per decade. Excitation voltages from 100 to 200 mV were applied. The measurements were carried out at temperatures between 693 and 818 K under various nitrogen/oxygen/butane ratios at a constant gas flow of 60 ml/min. The gas compositions were analysed on-line with an Agilent GC 6890 gas chromatograph. The oxygen impurity in nitrogen was ≤0.007 vol%.

2.2. Characterisation of VPO before and after operation in the EMR

2.2.1. Surface area

BET surface areas were measured with a Quantachrome Instruments Nova 2200 analyser, using N_2 as adsorbent at 77 K. Before the measurements, the samples were pretreated at 393 K for 48 h under vacuum in order to desorb impurities from the surface. The surface area was calculated from 5 adsorption isotherm points at relative nitrogen pressures (p/p_0) between 0.05 and 0.3.

2.2.2. X-ray diffraction (XRD)

The crystal structures of the presursor and catalyst samples were analysed with an X'Pert powder diffractometer using CuK_α radiation (40 kV, 40 mA) over the scan range from 10° to 80°. The angle step width was 0.167°, the counting time at each angle 30 s. The ICSD standard spectra library was used to identify the crystal phases present in the samples.

2.2.3. X-ray photoelectron spectroscopy (XPS)

After operation in the electrochemical membrane reactor, the VPO samples were collected from the membrane surface under dry nitrogen atmosphere in a glove box and transferred under nitrogen to a multipurpose UHV surface analysis apparatus (SPECS, Germany) for the XPS analysis of the vanadium oxidation state. A possible vacuum-induced reduction of the VPO samples was minimised by fast sample transfer times of less than 5 min between the start of the evacuation of the load lock and the first XPS spectrum at a pressure better than 5×10^{-9} mbar [14]. The X-ray source ($Mg–K_\alpha$, excitation energy 1253.64 eV, operation power < 200 W) was used in a "stop-and-go" mode in

order to reduce possible damage due to sample irradiation. High-resolution spectra (pass energy 10 eV, step size 0.1–0.2 eV) were recorded with a hemispherical energy analyzer (PHOIBOS-150, SPECS), which provides the possibility of simultaneous photo-electron detection on 9 channels, and allows fast data acquisition times (0.5 s per data point) with satisfactory signal-to-noise ratio.

Position-resolved XPS measurements were carried out in order to determine the spatial distribution of the vanadium oxidation states in the catalytic VPO layer used in the EMR.

2.2.4. Temperature programmed oxidation (TPO)

The temperature programmed oxidation (TPO) measurements were preformed using a BEL-CAT Catalyst Analyzer (Bel, Japan). The catalyst samples (50 mg) were pretreated under helium flow at 333 K for 10 min. During the TPO measurement the samples were heated from 333 to 900 K at a rate of 12 K/min under 4.0 vol% O_2 in helium with a total flow rate of 25 ml/min. Consumption and release of oxygen were monitored using a thermal conductivity detector (1 s per data point).

3. Results and discussion

3.1. Conductivity of the VPO catalyst

3.1.1. Impedance spectra

The conductivity of the VPO catalyst was measured during the activation under butane/oxygen atmosphere, and as a function of oxygen concentration and temperature. Figure 2 illustrates examples of EIS spectra from the activated VPO catalyst at temperatures of 693, 793 and 818 K under nitrogen atmosphere. Only one single semi-circle crossing the origin of the complex plane and touching the resistance axis at the low frquency side is observed in the Nyquist plot. The experimental impedance data were fitted to a simple equivalent circuit of a constant phase element (CPE, $1/C(j\omega)^{\alpha}$) and an ohmic resistance R connected parallel to each other. The frequency exponent α of the CPE was between 0.95 and 1.0, so the cell behaviour was close to that of a parallel-connected ideal capacitor and ohmic resistance. The electrical conductivity σ of the VPO was calculated from the resistance R via $\sigma = R^{-1} \cdot d \cdot A^{-1}$, where d is the thickness of the disc and A is the electrode area.

3.1.2. VPO conductivity under nitrogen and reaction gas atmospheres

During the initial VPO activation the conductivity was followed by recording impedance spectra in intervals of a few minutes. Figure 3 presents the total conductivity of VPO as a function of time during the activation. After an initial slight decay during the first hour of activation, the conductivity approached a constant value of about $\sigma = 10^{-6}\ \Omega^{-1}\ cm^{-1}$. After the activation period, the reaction gas (butane/air) mixture was replaced by nitrogen, and the conductivity dropped immediately by more than two orders of magnitude to $\sigma = 7\times\ 10^{-9}\ \Omega^{-1}\ cm^{-1}$. After renewed exposure of the VPO catalyst to the reaction gas, the initial conductivity level was reached again. By repeated change of the atmosphere between butane/air and nitrogen, the conductivity was found to switch reproducibly between these two levels. It should be noted, that the conductivities reported here have to be understood as effective values for pressed VPO powder, with contributions from the VPO itself as well as from grain boundaries.

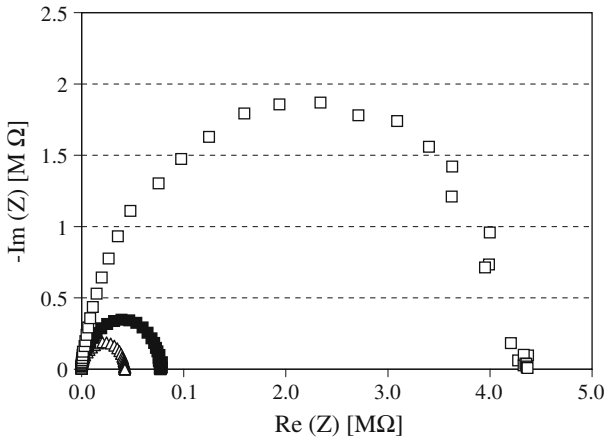

Figure 2. AC impedance response of activated VPO in a Pt/VPO/Pt disc (cell constant d/A = 0.16 cm^{-1}) at open circuit voltage in nitrogen atmosphere at (□) 693 K, (■)793 K and (Δ) 818 K. Applied exitation voltage 200 mV.

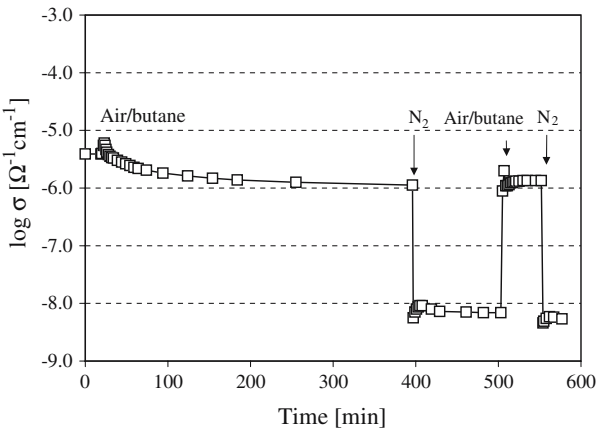

Figure 3. Total conductivity of VPO over time during the catalyst activation with butane (1.5 vol% in air) under nitrogen atmosphere at 693 K.

3.1.3. Temperature dependence

After the VPO activation, the temperature dependence of the conductivity was investigated under air as well as nitrogen atmosphere in the range from 718 to 818 K. The well reproducible reversibility of σ for increasing and decreasing temperatures indicated stability of the VPO material under the chosen conditions. The conductivity in air was several orders of magnitude higher than that under nitrogen. As expected, it increased with increasing temperature in both atmospheres, as illustrated in figure 4. Assuming that the conductivity follows the Arrhenius temperature dependence:

$$\sigma = \sigma_0 \exp(-E_A/kT) \quad (1)$$

with σ being the conductivity, the pre-exponential factor, E_A the activation energy and T the temperature, an activation energy of 1.60 eV is obtained for VPO in air. Under nitrogen atmosphere, in turn, the activation energy is 1.20 eV. The observed temperature dependence is more pronounced for the investigated VPO phase than for other vanadium phosphate phases since the obtained activation energies for VPO are clearly higher than those reported in the literature for the α_I-$VOPO_4$, β-$VOPO_4$, γ-$VOPO_4$ and δ-$VOPO_4$ vanadium phosphate phases, which were found between 0.40 and 0.85 eV [15].

3.1.4. Influence of the oxygen partial pressure

Finally, the conductivity was determined as a function of oxygen partial pressure in the range from 7 Pa to 20.8 kPa at 718 K. A substantial increase of the conductivity from 9.3×10^{-9} to $4.0\times 10^{-6}\ \Omega^{-1}\ cm^{-1}$ was observed between 7 Pa and 1.1 kPa. Further increase of the oxygen pressure leads to a less pronounced increase in conductivity, the highest value being $2.1\times 10^{-5}\ \Omega^{-1}\ cm^{-1}$ at 21 kPa. This behaviour is in qualitative agreement with a study by Herrman *et al.* who reported the dependence of the VPO conductivity on the exposing atmosphere, where the exposure to butane, with its reducing influence, decreased the conductivity remarkably compared to the one in air [16].

An increasing conductivity with increasing oxygen partial pressure is typical for *p*-type conducting oxides [17]: as the oxygen pressure is increased, extra oxygen entering the lattice in ionic form creates a deficiency of electrons, i.e., produces electron holes. The total electrical conduction consists generally from an electronic (σ_e) and an ionic (σ_i) contributions. Assuming here that the conductivity has an oxygen-dependent as well as an oxygen-independent contribution, the following equation can be fitted to the experimental data:

$$\sigma = \sigma_e + \sigma_i = K p_{O_2}^n + \sigma_{ind}. \quad (2)$$

The exponent n as well as the coefficients K and σ_{ind} in equation 3 were estimated by minimizing the weighted sum of residual squares between the experimental and the calculated conductivity. The procedure without constraints gave a value of 0.5 for n, and values of 1.60×10^{-7} and -4.06×10^{-7} were obtained for the parameters K and σ_{ind}, respectively. As can be seen from figure 5, the line intercepts the conductivity axis almost at zero, indicating a negligible conductivity (ionic as well as electronic) σ_{ind} under oxygen-free conditions.

For the conductivity of metal oxides, and depending on the conduction mechanism and the prevailing conditions, typically values of 0.25 or 0.17 have been reported for the exponent n, well below the value found in the present study [17–20]. Based on experimental data obtained here one can only state that the observed conduction in VPO cannot simply be described with the typical conduction models and so far no convincing

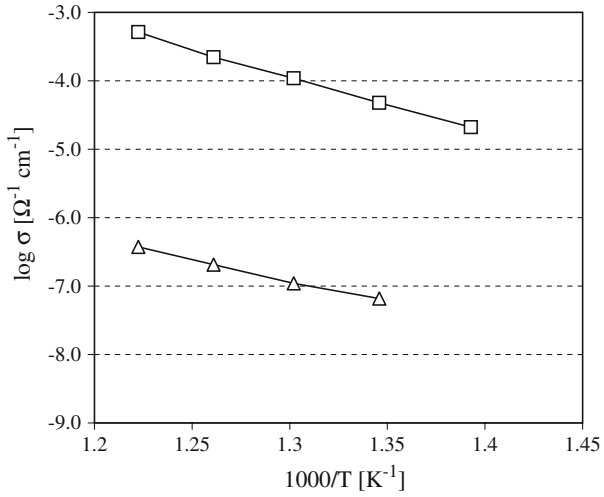

Figure 4. The total conductivity of the activated VPO as a function of temperature (□) in air and (Δ) in nitrogen atmosphere.

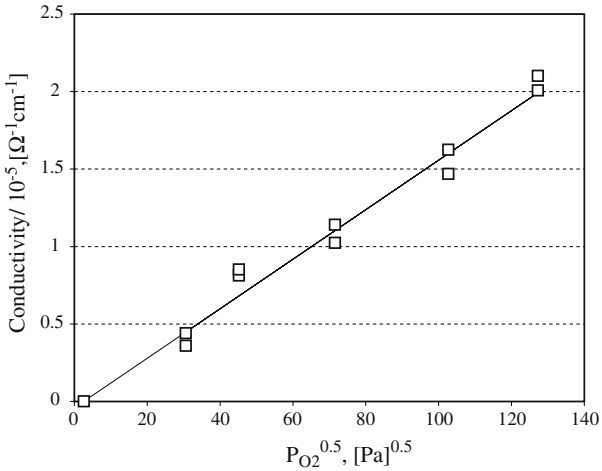

Figure 5. The total conductivity of the activated VPO as a function of oxygen partial pressure at 718 K. Inert gas nitrogen, total flow 60 ml/min.

explanation can be given for the observed exponential term of 0.5. However, the conductivity obtained here for VPO was several orders of magnitude lower than that of the investigated metal oxides [17–20] under all investigated conditions, and therefore a detailed experimental separation of ionic and electronic conduction is not relevant.

In commercial production processes of MA, the VPO catalyst is exposed to high oxygen concentrations, where diluted butane (below 1.5 vol%) is converted to MA. In our EMR application, however, the catalyst is fixed on the electrolyte membrane in the anodic compartment, where the oxygen is supplied in a very low concentration. We have shown before [9,10,21,22], that under these conditions part of the transported oxygen ions is converted neither to MA nor to CO_2 or CO, but is recombined to gaseous dioxygen. Due to these parallel processes, the oxygen concentration in the anodic compartment can vary, which in turn might influence the conductivity.

Summarizing the conductivity investigations it can be stated that the VPO catalyst shows an extremely low conductivity at low oxygen partial pressure, which is the prevailing condition in the anodic compartment in an EMR. Thus it can be concluded here, that the catalyst material VPO itself does not fullfill the requirements of being a sufficiently electronic or ionic conducting material in the anodic electrode layer. In order to have an efficient EMR operation, additional electronic and ionic conductors are necessary on the anodic side of the reactor.

3.2. Comparison of the fresh and used VPO catalyst

3.2.1. Surface area

The BET surface area of the precursor was 4 m^2/g which is somewhat lower than that reported by Kiely *et al.* (11 m^2/g) for a catalyst synthesised via the organic route [23]. For the freshly activated catalyst we obtained an increased surface area of 11 m^2/g, in close agreement with their data (14 m^2/g). Operation in the EMR reduced the surface area to values between 4 and 7 m^2/g.

3.2.2. X-ray diffraction

Figure 6 shows X-ray diffractograms (XRD) of the precursor, the freshly activated as well as the used catalyst, demonstrating that all the samples were well crystallised. For the precursor, all major diffraction peaks can be attributed to $VOHPO_4 \cdot 0.5H_2O$. After the activation, the precursor was completely converted to the activated VPO (see figure 6b), and all main peaks could be indexed to the $(VO)_2P_2O_7$ structure. The XRD analysis revealed that the bulk phase structure changed slightly during the EMR operation, since the diffraction peaks of the used catalyst in the XRD pattern showed less ordered structure than in the fresh, activated catalyst (compare peak intensities and widths in diffractograms b and c in figure 6).

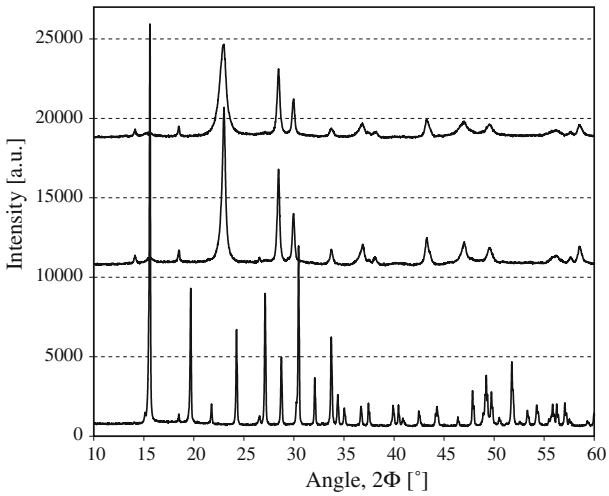

Figure 6. XRD diffractograms of (a) the precursor $VOHPO_4 \cdot 1/2H_2O$, (b) freshly activated $(VO)_2P_2O_7$ and (c) $(VO)_2P_2O_7$ catalyst which has been used in the electrochemical membrane reactor.

3.2.3. X-ray photoelectron spectroscopy (XPS)

The XPS-investigations reported herein were aimed towards two goals: first, the determination of the vanadium oxidation state for the different catalyst samples, and, secondly, the mapping of the spatial distribution of the V^{n+} ($n > 2$) species for both the inner and outer side of the tubular VPO layer used in the EMR (see figure 1). Since controversial interpretations of the right broad $V2p_{3/2}$ photoelectron peak as well as somewhat contradictive values for the binding energies for the V^{n+} contributions can be found in the literature, $VOPO_4$ with phase structure confirmed by XRD was used to calibrate the binding energy of the reference $V2p_{3/2}$ (V^{5+}) peak. The measured value of 518 eV (and the independently obtained value of 516.9 eV for V^{4+}

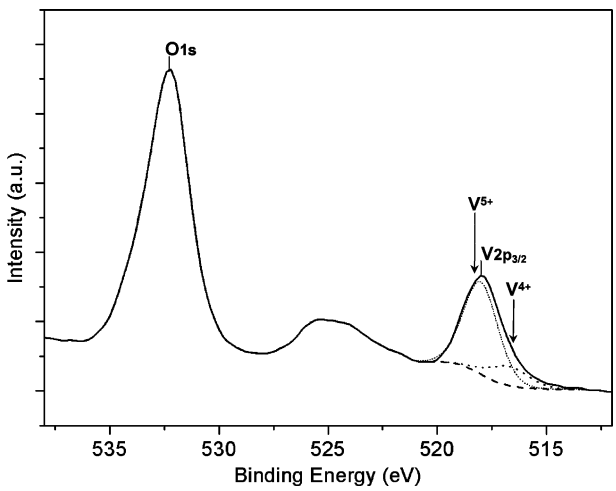

Figure 7. The O 1 s, $V2p_{1/2}$ and $V2p_{3/2}$ photoelectron peaks of a fresh VPO catalyst. Deconvolution of the $V2p_{3/2}$ peak in V^{5+} (518.0 eV) and V^{4+} (516.9 eV) contributions is also shown.

[14]) are in a good agreement with the literature [12,24,25], and were used for the $V2p_{3/2}$ peak deconvolution for all samples studied herein. As an example, a high resolution XPS spectrum containing the O 1 s, $V2p_{1/2}$ and $V2p_{3/2}$ photoelectron peaks for a fresh, activated VPO sample is shown in figure 7. Also shown is the corresponding deconvolution of the $V2p_{3/2}$ peak. Both V^{5+} and V^{4+} contribute with 82% and 18%, corresponding to a formal effective vanadium oxidation state of 4.82 for this sample. This value is somewhat higher than those previously reported in the literature for a fresh, activated catalyst [26,27]. We note, however, that the present data result from a "fast transfer" XPS i.e., are recorded after minimised exposition of the sample to the ultra high vacuum (UHV) conditions. We have shown before that vanadyl pyrophosphate samples can be remarkably reduced even during the first 10s of minutes of exposure to UHV [14]. Most of the published data were presumably collected under such circumstances.

For the second goal, position-resolved measurements have been performed, and axial (along the tubular reactor) as well as azimuthal distributions of V^{n+} species in the VPO layer were measured. The corresponding results are summarised in figure 8, where the effective oxidation state along the (axial) reactor coordinate for both radial positions – the inner (facing the YSZ membrane) and the outer (facing the anodic compartment with the butane) side of the VPO layer is plotted. The graph shows a remarkable reaction-induced difference in the oxidation state in the radial direction (i.e., across the VPO layer) as well as slight variations of the oxidation state in the axial direction along the reactor coordinate. Only negligible deviations of the oxidation state in the azimuthal distribution were observed, as is to be expected for the cylindrical geometry. The lowest oxidation state (4.5) is measured for the outer sample surface, facing the anodic gas compartment, the highest (4.9) for the inner (electrolyte membrane) side. With respect to the initial oxidation state of the fresh catalyst of 4.8, this corresponds to a slight increase in the vanadium oxidation state for the catalyst surface facing the electrolyte membrane and a corresponding decrease for the surface facing the anodic gas compartment.

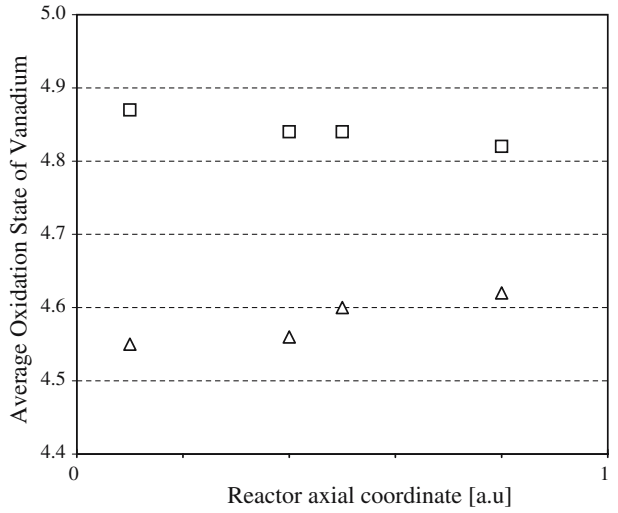

Figure 8. Distribution of the average oxidation state of vanadium in a VPO layer along the axial reactor coordinate in an EMR; (□) the surface facing the electrolyte membrane and (Δ) the surface facing the anodic compartment (gaseous butane).

These radial variations can be readily explained by the configuration of the EMR: the catalyst surface oriented towards the electrolyte membrane is in direct contact with the oxygen penetrating the membrane and thus exposed to an oxidizing atmosphere, while the catalyst surface facing the anodic gas compartment is exposed to the reducing hydrocarbon atmosphere. The axial variations on both sides of the catalytic layer correlate with the gas-inlet and – outlet positions in the EMR configuration (see figure 1) and are thus related to the geometry of reactant flows determined by the EMR design. The concentric symmetry of the reactant flows, expected from the EMR configuration, leads to the experimentally observed azimuthal symmetry in the oxidation state distribution.

In summary, we conclude here that in a membrane reactor where the reagents are brought separately to the catalyst layer, the local conditions and therefore the catalyst composition vary in a way, which can be readily understood on the basis of the reactor geometry and the reaction itself.

3.2.4. Temperature programmed oxidation (TPO)

In order to detect changes in the oxidation characteristics of the catalysts during EMR operation, TPO measurements were carried out for the fresh, activated catalyst and for the catalyst samples, which had been used in the EMR. The EMR operating conditions are rather reducing since the molar ratio of oxygen/hydrocarbon is typically well below one. The TPO graphs are presented in figure 9. Above the onset temperature of 866 K, the activated catalyst reacted with oxygen, which can be seen as a broad oxygen uptake (negative) peak with a maximum at 985 K in the TPO graph (see figure 7, line a). Surprisingly, further temperature increase caused a release of oxygen, which was detected as a positive peak with maximum at 1031 K. This unexpected release of oxygen under TPO conditions indicates, that we likely observe here a reversible uptake and release process of VPO catalyst lattice oxygen, rather than irreversible oxidation. A similar behaviour has been reported before for VPO catalysts in TPD measurements with various catalyst activation times in butane/air mixture [28,29]. During the oxygen TPD experiments Sakakini *et al.* observed the main oxygen desorption peak at 1023 K with a shoulder at 998 K, which they concluded to be due to the desorption of

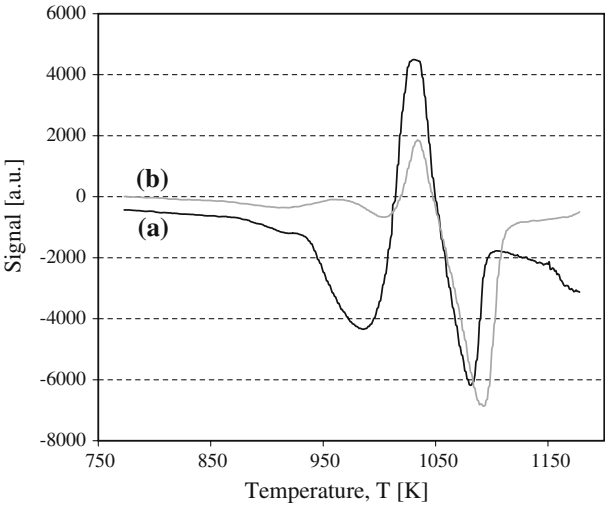

Figure 9. Temperature programmed oxidation (TPO) profiles of (a) the activated VPO, and (b) VPO used in an electrochemical membrane reactor. Heating rate 12 K/min to 1173 K, 25 ml/min, 4 vol% O_2 in He. Negative signal corresponds to oxygen consumption, positive one to oxygen release.

lattice oxygen [28]. Comparing the present TPO with the TPD results, we can state that their corresponding desorption temperature coincides well with our observations.

A qualitatively similar curve shape, as for the fresh one, was observed in the TPO graph of the used catalyst. However, a detailed analysis shows remarkable differences: firstly, the peak maximum temperature for the uptake of oxygen by the used catalyst was higher, at 1003 K, while the maxima of the oxygen release peaks are at approximately the same temperature for both samples. The second important point to note is the clearly lower amount of oxygen uptake and release from the used catalyst compared to that of the activated one. Based on an estimation of the peak areas the uptake by the activated catalyst is over 12 times that of the used one. During the subsequent oxygen release, the fresh, activated catalyst showed again higher activity, the oxygen release being about four times higher than that the used catalyst. These results clearly suggest that the ability of the used catalyst for oxygen uptake and release is lowered, which might explain in part the decrease of the selectivity to MA during several hours of operation. However, this conclusion is not easy to reconcile with the oxygen TPD results by Waugh and Taufiq-Yap, who observed a lowered oxygen desorption with catalyst owing higher selectivity after longer pretreatment time [29].

As the temperature was further increased, both the samples reacted further with oxygen, the peaks being at 1081 K and at 1092 K for the fresh and the used catalyst, respectively. The reaction in this temperature range is probably an irreversible oxidation, as was confirmed by a subsequent XRD analysis of both samples.

4. Conclusions

The observed very low conductivity under all investigated conditions suggests that additional electronic and ionic conducting components are needed in the anode composition in order to improve the operation in the EMR. X-ray diffraction analysis revealed that the crystallinity of the VPO decreased slightly during the operation in EMR, but that the $(VO)_2P_2O_7$ structure is still prevailing after extended time on stream. A remarkable reaction-induced difference in the vanadium oxidation states in the radial direction, and minor variations of the oxidation state in the axial direction along the reactor coordinate were observed by XPS, which can be understood on the basis of the reactor geometry and the separated reactant supply in EMR. The lowered selectivity of the catalyst after several hours of operation in the EMR is likely related to the observed decrease in the oxygen uptake/release property of the used VPO catalyst.

Acknowledgments

Financial support by the German Research Foundation (Deutsche Forschungsgemeinschaft) is gratefully acknowledged (research unit 447 "Membranunterstützte Reaktionsführung"). We thank Dr. Heike Lorenz, Max Planck Institute for Dynamics of Complex Technical Systems, for the XRD analysis.

References

[1] G.J. Hutchings, J. Mater. Chem. 14 (2004) 3385.
[2] M. Abon, J.M. Herrmann and J.C. Volta, Catal. Today 71 (2001) 121.
[3] X.S. Wang, L.J. Xu and X. Chen, J. Mol. Catal. A Chem. 206 (2003) 261.
[4] J.A. Lopez-Sanchez, L. Giresel, J.K. Bartley, R.P.K. Wells A. Liskoswki, D.S. Su, R. Schlögl, J.-C. Volta and G.J. Hutchings, Phys. Chem. Chem. Phys. 5 (2003) 3525.
[5] R.M. Conractor, Chem. Eng. Sci. 54 (1999) 5627.
[6] R. Mallada, M. Menendez and J. Santamaria, Appl. Catal. A: Gen. 231 (2000) 2489.
[7] R. Mallada, N. Pedernera, N. Menendez and J. Santamaria, Ind. Eng. Chem. Res. 39 (2000) 620.
[8] K. Sundmacher, L.K. Rihko-Struckmann and V. Galvita, Catal. Today 104 (2005) 185.
[9] Y. Ye, L. Rihko-Struckmann, B. Munder, H. Rau K. Sundmacher, Ind. Eng. Chem. Res. 43 (2004) 4551.
[10] Y. Ye, L. Rihko-Struckmann, B. Munder and K. Sundmacher, Appl. Catal. A: Gen. 285(1–2) (2005) 86.
[11] Y. Ye, Dissertation, Otto-von-Guericke University Magdeburg, Magdeburg 2005, in preparation.
[12] S. Albonetti, F. Cavani, F. Trifiro, P. Venturoli, G. Calestani, M. López Granados and J.L. Fierro, J. Catal. 160 (1996) 52.

[13] J.W. Johnson, D.C. Johnston, A.J. Jacobson and J.F. Brody, J. Am. Chem. Soc. 106 (1984) 8123.
[14] Y. Suchorski, L. Rihko-Struckmann, F. Klose, Y. Ye, M. Alandjiyska, K. Sundmacher and H. Weiss, Appl. Surf. Sci. 249 (2005) 231.
[15] F. Rouvet, J.-M. Herrman and J.-C. Volta, J. Chem. Soc. Faraday Trans. 90 (1994) 1441.
[16] J.-M. Herrmann, P. Vernoux, K.E. Béré and M. Abon, J. Catal. 167 (1997) 106.
[17] H.J.M. Bouwmeester and P.J. Gellings, in: *The CRC Handbook of Solid State Electrochemistry*, eds. P.J. Gellings and H.J.M. Bouwmeester (CRC Press, New York, 1997) ch. 1.
[18] T. Tsuju, Y. Maeda and Y. Yamamura, J. Phys. Chem. Solids 66 (2005) 339.
[19] M. Takahashi, Y. Noguchi and M. Miyayama, Solid State Ionics 172 (2004) 325.
[20] W. Wang and A.V. Virkar, J. Power Sources 142 (2005) 1.
[21] B. Munder, Y. Ye, L. Rihko-Struckmann and K. Sundmacher, Catal. Today 104 (2005) 138.
[22] Y. Ye, L. Rihko-Struckmann, B. Munder and K. Sundmacher, J. Electrochem. Soc. (2006) (in press).
[23] C.J. Kiely, A. Burrows, S. Sajip, G.J. Hutchings, M.T. Sanares, A. Tuel and J.-C. Volta, J. Catal. 162 (1996) 31.
[24] M. Abon, K.E. Bere, A. Tuel and P. Delishere, J. Catal. 156 (1995) 28.
[25] P. Delishere, K.E. Bere and M. Abon, Appl. Catal. A: Gen. 172 (1998) 295.
[26] N. Harrouch Batis, H. Batis, A. Ghorbel, J.C. Vedrine and J.C. Volta, J. Catal. 128 (1991) 248.
[27] M.P. Casaletto, L. Lisi, G. Mattogno, P. Patrono, G. Ruoppolo and G. Russo, Appl. Catal. A: Gen. 226 (2002) 41.
[28] B.H. Sakakini, Y.H. Taufiq-Yap and K.C. Waugh, J. Catal. 189 (2000) 253.
[29] K.C. Waugh and Y.H. Taufiq-Yap, Catal. Today 81 (2003) 215.